Vibration Serviceability Assessment for Pedestrian Bridges Based on Model Falsification

Wen-Jun Cao [1], C. G. Koh [2] and I. F. C. Smith [3]

[1] Ph.D., Researcher, ETH Zurich, Future Cities Laboratory, Singapore-ETH Centre, # 06-01, CREATE Tower, 1 Create Way, 138602, Singapore (corresponding author). E-mail: caowenjun@u.nus.edu
[2] Professor, Department of Civil and Environmental Engineering, National University of Singapore, 1 Engineering Drive 2, 117576, Singapore. E-mail: cgkoh@nus.edu.sg
[3] Professor, Applied Computing and Mechanics Laboratory (IMAC), School of Architecture, Civil and Environmental Engineering (ENAC), Swiss Federal Institute of Technology (EPFL), GC G1 507, Station 18, CH-1015, Lausanne, Switzerland. E-mail: Ian.Smith@epfl.ch

Abstract:

With the development of new materials and advanced structural analysis, alongside increasing aesthetic requirements, recent years have witnessed a trend towards longer, taller, and lighter footbridges. Different from vehicular bridges, footbridges carry relatively small service loads and are more susceptible to vibrations due to their lower stiffness, damping, and modal mass. More often than not, vibration serviceability limit state governs the design of footbridges. To provide an accurate evaluation of vibration serviceability performance of existing bridges requires techniques that can include modeling and measurement uncertainties. In this paper, a population-based method called error-domain model falsification (EDMF) is used to assess the vibration serviceability for two pedestrian bridges: Fort Siloso Skywalk located in Singapore and the Dowling Hall footbridge located at Tufts University in the United States. The unknown properties of the footbridges are identified using the ambient vibration data measured on site. This method is also compared with two other data-interpretation methodologies, i.e., residual minimization and traditional Bayesian model updating. The findings show that, through explicitly accounting for measurement and modeling uncertainties, EDMF can provide more accurate identification and prediction results for vibration serviceability assessment of pedestrian bridges.

Keywords:

Model falsification, vibration serviceability limit state, full-scale test, pedestrian bridge

Introduction

According to the Institution of Structural Engineers' 2015 survey, 49% out of 27,000 footbridges throughout the world have experienced vibration serviceability problems, while 23% received complaints regarding human comfort (Brownjohn and Darby 2018). This is because slender footbridges usually have one or more natural frequencies that lie within the dominant spectrum of common human activities such as walking, running, or jumping (Catbas and Kijewski-Correa 2013). As a result, footbridge design is often governed by vibration serviceability limit state rather than the ultimate limit state. The fundamental method is to avoid structural natural frequencies being within the ranges associated with pedestrian pacing or to ensure the acceleration levels of the footbridge below prescribed acceptable limits. For example, in EN 1990/A1 (*EN 1990:2002/A1:2005 Eurocode—Basis of structural design. Application for bridges* 2005), the vibration comfort criteria require that the fundamental frequency of the footbridge shall be less than 5.0 Hz for vertical vibrations and 2.5 Hz for horizontal and torsional vibrations.

Finite element models are widely used to analyse and predict structural behaviour. However, due to modelling simplifications and assumptions on unknown structural system properties (e.g., boundary conditions, material and geometric properties) and deviation introduced in the construction phase, the model used in the design phase is not an accurate representation of the built system. Unlike spacecraft, nuclear power plants and wind farms, footbridges are rarely subjected to experimental validation of design models. Therefore, to better predict the real behaviour of footbridges, vibration serviceability should be evaluated using the models updated by on-site measurements and inspections.

In the application of monitoring footbridges, full-scale measurements can be categorized into two types (Feldmann et al. 2010). Type I refers to the dynamic responses obtained under deliberate loading (e.g., jumping, jogging and horizontal body swaying of one person or a group of people). This type of data can be used to directly assess human comfort level for excitation events. Type II refers to the vibration data obtained from ambient vibration tests, free vibration tests and forced vibration tests. This vibration data can be used to identify modal properties (e.g., natural frequencies and mode shapes).

For vibration-based structural identification and response prediction, a 'three-stage' approach (Brownjohn et al. 2011; Byfield and Paramasivam 2012) has been commonly used given the difficulty of identifying unknown model parameters directly from vibration data. In Stage I, modal properties are identified using Type II measurements. Those identified properties are then used as "indirect measurements" in the structural identification in Stage II. Responses are predicted based on the updated models (the output of Stage II) in Stage III.

Structural identification (or model updating) can be achieved through the modification of modeling assumptions and tuning model parameters until the model predictions agree well with the results of on-site tests based on a trial and error approach (Mottershead et al. 2011) (Ren and Peng 2005). However, this approach is not efficient and may not guarantee an accurate identification. A commonly adopted procedure is residual minimization to find the parameter values that yield the "best match" with measurements. The task is posed as an optimization problem whereby the objective function is the weighted sum of discrepancies between model predictions and test measurements. For example, Araujo et al. (Araujo et al. 2011) computed the modal properties from the ambient vibration data using the Eigensystem Realization Algorithm (ERA). Then they used genetic algorithm to solve the optimization task to find the optimal parameter values using identified modal properties. However, the formulation of the objective function is difficult. A popular approach is to assign weighting factors to each of the dynamic characteristics including natural frequencies and mode shapes (Friswell et al. 1998). Kim and Park (Kim and Park 2004) introduced multi-objective functions to extremise several objective terms simultaneously.

Probabilistic finite element model (FEM) updating using Bayesian inference schemes has been proposed since the 1990s. This method uses Bayesian conditional probability to update the prior knowledge of model parameters using measurements and inspection (Beck and Katafygiotis 1998; L. S. Katafygiotis; J. L. Beck 1998). Many applications on bridges can be found in the literature, for example, (Cheung and Beck 2009, 2010; Yuen et al. 2004, 2006). Lam et al. (Lam et al. 2015) carried out Bayesian model updating of a coupled-slab system using an ambient vibration test. Yin et al. (Yin et al. 2010) detected cracks in thin plate structures using a Bayesian approach based on dynamic responses at only a few points on the plate. Zheng and Yu (Zheng and Yu 2013) assessed the structural integrity of scoured bridges based on vibration-based measurements. In a similar way to residual minimization, Bayesian model updating requires the assignment of relative weighting factors to the contributions of the mode shape vectors and modal frequencies in the likelihood function (Goller et al. 2012).

Goulet et al. (Goulet et al. 2010) proposed another methodology named error-domain model falsification (EDMF). They then demonstrated the applicability of this approach for structural identification and performance monitoring of real structures by applying it to Langensand Bridge in Switzerland. The predictions from the set of candidate model instances reveal a reserve capacity of 30% with respect to serviceability requirements (Goulet et al. 2010).

To obtain a better understanding of prediction uncertainties, Goulet et al. (Goulet et al. 2014) investigated the Grand-Mere Bridge located in Canada and discovered that model simplification has an important influence on prediction errors. This approach also provides a less conservative estimate of the remaining fatigue life and reveals that traffic models and structural model parameters are the most influential sources of uncertainty (Pasquier et al. 2016). This method has also been applied in optimal sensor placement by Papadopoulou et al. (Papadopoulou et al. 2016) and Bertola et al. (Bertola et al. 2017), leak detection in pipe networks by Moser et al. (Moser et al. 2018) and wheel-flat detection in the train-track system by Cao et al. (Cao et al. 2019b).

Although there are comparison studies of various system-identification methodologies, the performance of these three methodologies (EDMF, residual minimization, and traditional Bayesian model updating) has not been studied in the scope of vibration serviceability assessments.

This paper presents the vibration serviceability assessments of two footbridges: Fort Siloso Skywalk in Singapore and Dowling Hall Footbridge inside Tufts University campus. In each case study, the three methodologies are compared in terms of their performance for diagnosis and prognosis.

Background: System identification methods

Residual minimization

Residual minimization, also known as model calibration, involves finding the optimal parameter values ($\hat{\boldsymbol{\theta}}$) by adjusting the parameters ($\boldsymbol{\theta}$) so that the finite element predictions best match the measurements. A commonly used function is the sum of the squares of the differences between predicted ($\mathbf{g}(\boldsymbol{\theta})$) and measured values ($\boldsymbol{y}$), the number of measurements is denoted as n_m.

$$\hat{\boldsymbol{\theta}} = \underset{\theta}{\mathbf{argmin}} \sum_{i=1}^{n_m} (\mathrm{g}_i(\boldsymbol{\theta}) - y_i)^2 \tag{1}$$

Bayesian model updating

Probabilistic finite element model updating using Bayesian inference has been proposed since the 1990s. This method uses Bayesian conditional probability to update the prior knowledge of model parameters using measurements and inspection (Beck and Katafygiotis 1998; L. S. Katafygiotis; J. L. Beck 1998). The prior probability of physical parameters $P(\boldsymbol{\theta})$ is updated using a likelihood function $P(\mathbf{y}|\boldsymbol{\theta})$ and measured data **y.** The posterior probability $P(\boldsymbol{\theta}|\mathbf{y})$ is obtained using the normalization constant $P(\mathbf{y})$.

$$P(\boldsymbol{\theta}|\mathbf{y}) = \frac{P(\mathbf{y}|\boldsymbol{\theta})P(\boldsymbol{\theta})}{P(\mathbf{y})} \tag{2}$$

Instead of searching for only one solution (maximum a posteriori) as residual minimization, this approach can also estimate the level of confidence of identified results. This approach may include a covariance matrix to describe the uncertainty variances and correlation coefficients for each measurement. In this paper, the traditional Bayesian model updating (tBMU) employing a zero-mean Gaussian distribution for uncertainty is used for comparison purpose.

Error-domain model falsification

Error-domain model falsification samples thousands of models from a general parametrized model in which the initial parameter domain is defined by engineering judgment and preliminary knowledge. A model is accepted when it is supported by evidence (measurements or inspections) and conversely, falsified when it is not consistent with evidence.

The falsifying criteria are based on “rectangular” threshold bounds, which are determined by the combination of modeling and measurement uncertainties. For one model instance, if any residual value between the prediction and the measurement falls outside the threshold bounds, this model instance is falsified. If the residual values of all comparison points are inside the threshold bounds, it is considered a candidate model instance. Candidate model set (CMS) are considered “acceptably correct” according to the current information provided by measurements and inspections. With more information added, however, some or even all of the current candidate models may be further falsified.

Let n_m be the number of measurements and assume we have already obtained the candidate parameter values, denoted as $\boldsymbol{\theta}^*=[\theta_1^*,\theta_2^*,\cdots,\theta_n^*]^T$, where n is the number of parameters. For measurement i, the addition of the prediction response $g_i(\boldsymbol{\theta}^*)$ calculated by finite element analysis and modeling uncertainty $\epsilon_{model,i}^*$ should be equal to the true response $\mathcal{T}$, which should also be equal to the addition of measurement y_i and measurement uncertainty $\epsilon_{meas,i}^*$ (Equation (3)). By rearranging both uncertainties in the right-hand side of the Equation, Equation (4) is obtained. For a candidate model, the difference between $g_i(\boldsymbol{\theta}^*)$ and y_i should fall inside the threshold calculated by the combined uncertainty $U_{c,i}$.

$$g_i(\boldsymbol{\theta}^*) + \epsilon_{model,i}^* = \mathcal{T} = y_i + \epsilon_{meas,i}^* \tag{3}$$

$$g_i(\boldsymbol{\theta}^*) - y_i = U_{c,i} \tag{4}$$

Let ϕ be the target confidence level and $F_{U_{c,i}}^{-1}(x): x \in [0,1]$ represent the inverse cumulative distribution function of the combined uncertainty. The rectangular coverage region defined by threshold bounds $T_{low,i}$ and $T_{high,i}$ is found using the Šídák correction and a target reliability ϕ (Goulet and Smith 2013). ϕ is commonly set to be 0.95 in civil engineering (Pasquier and Smith 2016).

$$T_{low,i} = F_{U_{c,i}}^{-1}\left(\frac{1}{2}\left(1 - \phi^{1/n_m}\right)\right) \tag{5}$$

$$T_{high,i} = F_{U_{c,i}}^{-1}\left(1 - \frac{1}{2}\left(1 - \phi^{1/n_m}\right)\right) \tag{6}$$

In most applications, the modal assurance criterion (MAC) is adopted to estimate the degree of correlation between the simulated mode shape and the experimental mode shapes. It is introduced either into the objective function in residual minimization techniques or the Bayesian-based approach. MAC is a good statistical indicator to pair modes in conjunction with frequency comparison. However, for example, in full-scale structures, an objective function with a MAC value equal to 0.99 is not necessarily more consistent with real structural behavior than an objective function with a MAC value equal to 0.96. One of the reasons is that, in most finite element models, material properties, geometry and construction quality are considered to be homogeneous and boundary conditions are assumed to be the same for all support bearings. These assumptions do not hold for bridges in the built environment (Liu and Cheung 2020; Nguyen et al. 2013). In practice, values of MAC in excess of 0.8-0.9 can be accepted as indicators of good consistency (Rainieri and Fabbrocino 2014) (Brownjohn et al. 2003)(Goulet et al. 2013).

Case study I: Fort Siloso Skywalk

Bridge description

Fort Siloso Skywalk in Singapore is an eight-span continuous steel pedestrian bridge with a concrete deck on the surface (Figure 1). The layout of the bridge is an ‘S’ curve and the total length is about 181m. The typical intermediate span is 23.5m and the end span is 20m. One end of the bridge ties to the 38m-height tower while the other end connects to the elevated ground. The width of the bridge is 3.0m.

Vibration tests and analysis

To measure the dynamic response of this pedestrian bridge, accelerometers (PCB393B12 with sensitivity of 10V/g and broadband resolution of 8μg) were installed at three locations (A, B and C) on the surface of the concrete deck along one side of the bridge (Figure 2). At each location, three uniaxial accelerometers were used to record the vertical/transversal/longitudinal responses at a sampling rate of 1024Hz. The signals were resampled to 256Hz for data processing.

The vibration tests include the following three types of events:

Event I: Vertical and lateral jumping of a small group of people to estimate the damping ratio of the bridge using the free decayed data.

Event II: Ambient vibration (with no human activity) to measure the natural frequencies.

Event III: Random walking test involving 40 people.

The reason that the damping ratio of the bridge is extracted using Event I instead of Event II is because the damping ratio is amplitude-dependent. Damping ratios obtained through ambient vibration are usually at least an order of magnitude lower than the serviceability level (Au 2017).

Vertical and lateral jumping

On each span, ten persons were asked to jump (vertically and laterally) and to then remain still after the jump, causing a free decayed vibration phase. The free decayed signals are used to estimate the damping ratios in the vertical direction and horizontal direction, respectively.

The accuracy of damping ratio depends on the quality of decayed vibration signal which, in turn, depends on the synchronization of individuals in jumping and any disturbance due to human movement after the jump. Assuming that the free vibration response generated by jumping is dominated by a single vibration mode, the peak amplitudes (A_i) of successive cycles in the decayed vibration can be approximated by the following equation:

$$A_i = A_0 \exp[-2\pi\zeta i] \tag{7}$$

where ζ is the damping ratio. The above equation can be written as follows:

$$\ln(A_i) = \ln(A_0) - 2\pi\zeta i \quad (8)$$

The procedure for quantifying the damping ratios is as follows:

(1) For each span, by plotting $\ln(A_i)$ versus the number of cycles (i), a linear regression analysis is carried out to estimate the damping ratio from the negative slope divided by 2π. The derived damping ratios are shown in Table 1, whereby R^2 is the coefficient of determination that shows how well the data fit the linear regression model.

(2) The average damping ratio is determined by:

$$\zeta = (\zeta_A R_A^2 + \zeta_B R_B^2 + \zeta_C R_C^2)/(R_A^2 + R_B^2 + R_B^2) \quad (9)$$

The damping ratios in the vertical direction and horizontal direction are found to be 2.15% and 0.99%.

Modal analysis

In the ambient vibration test, vibration data from nine accelerometers were recorded for 4 minutes when there was no human activity on the bridge. Bayesian operational modal analysis (BAYOMA) (Au 2012a; b) is used to analyze the data. In addition to providing the most probable estimate of modal properties, BAYOMA is able to quantify the associated uncertainty.

Figure 3 (a) shows the computed power spectral density (PSD) using the recorded data. The peaks in the PSD spectrum indicate potential modes. To provide a better vision of these modes, the corresponding singular-value (SV) spectrum is calculated and presented in Figure 3 (b). The hand-picked initial guesses and frequency bands are listed in Table 2. A total of 12 modes are identified. Their most probable values (MPV) of natural frequencies and their corresponding coefficient of variation (COV) are summarized in Table 3.

Structural identification

The footbridge is modeled in ANSYS (ANSYS 2016) (Figure 4). The concrete deck is modeled by a shell element while the steel element is modeled by a beam element. The main member of the girder is welded on to a steel plate which is embedded in the reinforced concrete beam of the tower. The connection between the tower and the foundation is modeled as fixed. The other end of the footbridge is simply supported by the elevated ground. For P1-P7, the boundary conditions of each pier are modeled by three linear springs in the vertical, transverse and longitudinal directions respectively.

In this case study, unknown parameters include Young's modulus of concrete and steel (E_C, E_S), the equivalent density of the deck and steel (D_C, D_E), logarithm of transversal stiffness of bearings (log T), logarithm of vertical stiffness of bearings (log V) and logarithm of longitudinal stiffness of bearings (log L), as listed in Table 4. The range of E_C is referenced from Cao et al. (2019a). The ranges of log T, log V, and log L are set based on pile and plate load tests as well as soil-structure interaction analysis used in the design. The range of E_S is set to be $\pm$ 5% lower and upper bounds around the nominal value (Pasquier et al. 2014). The ranges of D_E and D_C are set based on engineering judgment. Uniform distributions are assigned to the initial ranges of these parameters based on the principle of maximum entropy (Jaynes 2003).

Although 12 modes are detected through operational modal analysis, some of the measured mode shapes (only at location A-C) are not enough to match with the simulated ones using FEM (eight-span mode shapes). As a result, only six modes are paired based on MAC criterion between the measured and simulated mode shapes (shown in Figure 5).

Modeling and measurement uncertainties are summarized in Table 5. The measurement uncertainty related to modal analysis is taken from the study presented in the previous section

(Table 3). Additional uncertainty accounts for all other sources that individually have negligible influence, for example, round off of numbers (Goulet et al. 2010). Other uncertainties are estimated according to Cao et al. (2019a), Goulet (2012). Due to the lack of more detailed information, all uncertainties are assigned as uniform distributions based on the principle of maximum entropy. In EDMF, evaluation of existing structures usually requires an iterative falsification process because the selection of EDMF settings varies from case to case (Pasquier and Smith 2016). In the first trial, 1000 model instances generated by Latin hypercube sampling are calculated using finite element analysis. After falsification, 17 candidate models are obtained. In the second trial, 3000 model instances are calculated. After falsification, 62 candidate models are obtained. Increasing the sample size from 1000 to 3000, the ratio of candidate models remains approximately the same, i.e., about 2% of the initial model instances. If adding more model instances significantly changes the proportion of candidate models , a substantial increase in sample size is required. In this case study, since the proportion of candidate models has already converged, there is no need to increase the sample size. The trial using 3000 model instances is presented herein as the final result since it results in more candidate models. The identification results are presented in Figure 6 where each grey line represents an initial model instance, and each red line represents a candidate model. It is shown that only the ranges of E_C and log V are reduced after identification. This is because, in the test, accelerometers were installed only in the first three spans of the eight-span bridge due to practical constraints. Based on the limited information provided by measurements, EDMF is only able to reduce the ranges of two parameters.

Before proceeding to the vibration serviceability assessment using the candidate models, a validation is conducted to determine whether the structural identification is reasonable. Since the real parameter values are not available in full-scale structures, a cross-validation strategy is conducted.

Validation is carried out six times. Each time, one mode out of the six modes is held out from the measurement set and is assumed as unknown. Using the remaining five modes, EDMF is carried out to obtain the candidate models which are then used to predict the natural frequency of the "unknown" mode. The range of the real natural frequency of the "unknown" mode (ith mode) is obtained by adding the measured value y_i and the measurement uncertainty $\epsilon_{meas,i}$ (see the right-hand side of Equation (3)). If this range overlaps with the range that is obtained by adding the predictions $g_i(\boldsymbol{\theta})$ and the prediction uncertainty $\epsilon_{model,i}$ (see the left-hand side of Equation (3)), structural identification is considered to be validated. Otherwise, the identification is not successful. The cross-validation results for EDMF are summarized in Table 6 and presented in Figure 11. In Figure 11, the measurement uncertainty is highlighted as the grey area along with the measurement (black line). It is shown that in every scenario, the measurement falls within the prediction provided by EDMF (rectangular pink area). Thus EDMF is shown to be able to provide accurate identification results.

Vibration serviceability limit assessment

As shown in previous sections, the first lateral mode has a natural frequency of around 1 Hz and a modal damping ratio of 0.99%. The first vertical mode has a natural frequency of around 5 Hz and a modal damping ratio of 2.15%. According to Human Induced Vibrations of Steel Structures (HiVoSS) (Feldmann et al. 2010), for lateral vibration, the natural frequency falls into the critical range (0.5 Hz $\leq f_{1-lateral} \leq$ 1.2 Hz). A further assessment of maximum acceleration is required.

For each candidate model, a uniformly distributed harmonic load model $p(t)$ is applied to the bridge according to the critical lateral mode shape. $p(t)$ is calculated as follows (Feldmann et al. 2010):

$$p(t) = P\cos(2\pi f_s t)\, n'\Psi \qquad (10)$$

where P is the component of the force due to a single pedestrian with a walking step frequency f_s. For lateral calculation, P= 35 N. f_s = 1 Hz is the fundamental frequency of the lateral mode of the footbridge. n' is the equivalent number of pedestrians on the loaded surface. The values of n' and the reduction coefficient Ψ are taken from (Feldmann et al. 2010). For each candidate model, the maximum lateral acceleration under the harmonic force is calculated (Figure 7). Then, the modelling uncertainty (Table 7) is added to the candidate models' predictions, following Equation (3).

As mentioned in the previous section, the only available information of model parameters, modeling uncertainties, and measurement uncertainties are their lower and upper bounds. Uniform distributions are assigned to them through the principle of maximum entropy. In reality, it is very rare that more sophisticated distributions for dominant modeling uncertainties can be justified. For practical reasons, all values between the lower and upper prediction bounds have the same probability of occurrence. In this case study, the maximum acceleration obtained using EDMF is within the range of [0.0223 m/s^2, 0.0770 m/s^2] with a uniform distribution. The lateral comfort level of this bridge is comfort class CL1 which requires the lateral acceleration being smaller than 0.1 m/s^2. According to the design guideline (Feldmann et al. 2010), the lock-in phenomenon will be triggered if the lateral acceleration is within the range of [0.1 m/s^2, 0.15 m/s^2]. For this bridge, there is no such risk.

To verify the prediction accuracy, a random walking test was conducted (Event III). According to the design guideline, the pedestrian density is 0.5 P/m^2 based on pedestrian traffic class TC3 characterized by "still unrestricted walking; overtaking can intermittently be inhibited". About 35 people were scattered over an area of approximately 70 m^2 for the typical span of 23.5 m and width of 3 m. In this test, 40 people walked randomly in a group with no attempt to synchronize their walking pace (Figure 8). The peak values of the measured accelerations at

Point A, B and C and the corresponding comfort levels are summarized in Table 8. The maximum lateral acceleration is 0.079 m/s^2 based on 40 people walking in the test. Scaling down to 35 people as required in the design guideline, the lateral acceleration is approximately 0.069 m/s^2 which is within the predicted range by EDMF's [0.0223 m/s^2, 0.0770 m/s^2]. The comfort levels at all three measurement points on the bridge are CL1 which is the same as the model predictions.

Comparison with residual minimization and traditional Bayesian model updating

In residual minimization (RM), the optimal solution of parameters is obtained by minimizing the discrepancy between measurements and simulations. The objective adopted in this section is:

$$\hat{\boldsymbol{\theta}} = \underset{\theta}{\mathbf{argmin}} \sum_{i=1}^{n_m} (\mathrm{g}_i(\boldsymbol{\theta}) - y_i)^2 \tag{11}$$

where n_m= 6, $\mathrm{g}_i(\boldsymbol{\theta})$ and y_i are the natural frequency derived from FEM simulations and measurements respectively. The optimization is carried out using Adaptive Single-Objective method provided in Ansys Workbench (Lee 2018). This method combines an optimal space-filling design, a Kriging response surface and mixed-integer sequential quadratic programming (Exler and Schittkowski 2007). In Figure 9, the optimal solution is indicated by a blue dashed line.

In traditional BMU, the prior knowledge of the model parameters is updated based on Bayes' theorem. The uncertainty is assumed to have an independent zero-mean Gaussian distribution for each mode. For mode i, the standard deviation is $\sigma_i = (U_{upper} - U_{lower})/6$, where U_{upper} and U_{lower} are the upper and lower bounds of combined uncertainties used in EDMF. This ensures that the range of combined uncertainty falls within three standard deviations of Gaussian distribution, accounting for 99.7% values of the whole distribution. The Metropolis algorithm (Chib and Greenberg 1995) is used to estimate the posterior distribution. Specifically, the proposal distribution is a multivariate uniform distribution whereby in each dimension, the lower and upper bounds are set to be ± 1/20 of the total length of its initial parameter range (see Table 4). To reduce the correlation between samples in a Markov chain, As a burn-in period, samples between the starting point and 10,000th point are discarded in the generated sequence. The resulting posterior distributions of parameters are shown in blue histograms in Figure 9. In EDMF, each candidate model is assumed to have an equal probability of occurrence. The EDMF results are shown in the rectangular area in Figure 9.

Figure 10 presents the predictions of maximum acceleration using the three methods considered. Using the optimal parameter set obtained through RM, the maximum lateral acceleration under the harmonic lateral loads is 0.033 m/s^2, which is far below the acceleration obtained in the test (0.069 m/s^2). The 5th percentile and 95th percentile bounds of the acceleration predicted using traditional BMU are 0.0236 m/s^2 and 0.0702 m/s^2, which cover the acceleration obtained in the test. In summary, in this case study, EDMF and traditional BMU are able to provide predictions that are consistent with experimental observation whereas RM underestimates it.

The cross-validation test carried out for EDMF is also performed for RM and traditional BMU (tBMU). As shown in Figure 11, in Scenario 2 and Scenario 5, RM successfully predicts the natural frequency of Mode 2 and Mode 5. But in the remaining scenarios, the predictions are far away from the measurements. In all six scenarios, tBMU is able to provide accurate identifications of the "unknown" modes because the predictions by tBMU (blue histogram) overlap with the measurements (black lines) with the measurement uncertainties (grey areas). In this case study, both EDMF and tBMU are validated while RM fails to pass the validation test (Table 9).

Case study II: Dowling Hall footbridge

Bridge description

Dowling Hall footbridge is located at the Tufts University campus. It is a two-span footbridge connecting the Dowling Hall and the main campus. The steel frame footbridge is 44m long and 3.7m wide with a composite deck (concrete with wire-welded fabric and steel corrugated slab). The bridge is supported by an abutment on the campus side and pier structures at the center and at the Dowling Hall side. A continuous structural monitoring system is installed on this bridge; details can be found from (Moser and Moaveni 2013). Six vibration modes of the footbridge with natural frequencies of 4.68 Hz (vertical mode), 5.99 Hz (vertical mode), 7.16 Hz (torsional mode), 8.94 Hz (torsional mode), 13.19 Hz (vertical mode) and 13.73 Hz (vertical mode) are identified (Moser and Moaveni 2013).

Structural identification

In the finite element analysis using Ansys (ANSYS 2016), the composite deck is idealized as a concrete deck with equivalent weight and stiffness and modeled by Shell-181 elements. Shell-181 element is a four-node element with six degrees of freedom at each node. The steel members are modeled using Beam-188 element which is based on Timoshenko beam theory including shear deformation effects. The six vibration modes, which are paired with the experimental results based on MAC criterion, are identified in FEM simulations shown in Figure 12.

After sensitivity study, unknown parameters to be identified include Young's modulus of bridge deck (E), the equivalent density of bridge deck (D), the logarithm of vertical stiffness of the abutment support ($\log V_A$), the logarithm of vertical stiffness at the middle support ($\log V_M$) and the logarithm of longitudinal stiffness of the side support ($\log L_S$) (Table 10). The initial ranges of the stiffness of the supports are estimated based on a previous study (Moaveni and Behmanesh 2012). The range of D is set to be $\pm 15\%$ (engineering judgement) from the equivalent density calculated based on design drawings. The lower bound and upper bound of E is taken from (Cao et al. 2019a). The models and measurement uncertainties are summarized in Table 11. The modeling uncertainty is larger than the one used in the first case study (Fort Siloso Skywalk). This is because in the modeling of the Dowling Hall Footbridge, the composite deck (with wire-welded fabric and steel corrugated deck) is idealized as a concrete slab with equivalent weight and stiffness. The temperature effects on the natural frequencies have been studied by Moser and Moaveni (Moser and Moaveni 2013), where natural frequencies are seen to vary at most by 8% in the time period studied. Other uncertainties are referenced from (Cao et al. 2019a).

In the first trial of EDMF, 1000 model instances are generated using Latin Hypercube sampling in the parameter domain. EDMF results in 9 candidate models. In the second trial, the number of initial model instances is increased to 3000 and 27 candidate models are obtained. The proportion of candidate models has converged and thus the EDMF results based on 3000 model instances are presented. As shown in Figure 13, the vertical axes represent parameter values and predictions of natural frequencies. Each blue line represents a candidate model. The red area represents the threshold calculated for each natural frequency. The identified ranges of parameter values are listed in Table 12.

In a similar way to the first case study, the cross-validation process is conducted for Dowling Hall footbridge. For each scenario, the natural frequency of one mode is assumed to be unknown. Parameter values are identified using the rest of modes with EDMF. The evaluation is carried out by comparing the predictions provided by identified parameter values with the measurement of the "unknown" mode. The results are summarized in Table 13 and Figure 16.

It is shown that for all the six scenarios, the measured natural frequency for each "unknown" mode falls within the prediction bounds provided by EDMF. In this way, EDMF is again shown to be able to provide accurate identification of parameter values.

Vibration serviceability assessment

The design guide for vibration serviceability assessment jointly published by the American Institute of Steel Construction and the Canadian Institute of Steel Construction (Murray et al. 1997) is used for Dowling Hall Footbridge. The fundamental frequency of this bridge is larger than 3Hz, which meets the design guide. Unlike the first case study, only ambient vibration tests were carried out for this bridge. As a result, other vibration checks will follow the procedure in the design guide that provides vibration criteria for walking and rhythmic excitations. For this outdoor footbridge, only the peak acceleration under walking excitation has to be checked. Following the design guide, the peak acceleration due to walking is around 0.017g, which does not exceed the allowable acceleration of 0.05g. Hence, this footbridge is considered to have satisfied the vibration serviceability limit state.

The vibration serviceability assessment of this bridge is also carried out according to HiVoSS (Feldmann et al. 2010) as it provides a more detailed guideline than the USA practice. For Dowling Hall Footbridge, the natural frequency of vibration falls inside the range of 2.5Hz and 4.6Hz. This indicates that the bridge might be excited to resonance by the second harmonic of pedestrian load. Following the requirement in HiVoSS (Feldmann et al. 2010), a uniformly distributed harmonic load model vertical load $p(t)$ is applied to the bridge according to the critical vertical mode shape. For each candidate model, the maximum vertical acceleration under the harmonic force is calculated. As shown in Figure 15, EDMF's prediction is within the range of [0.109 m/s^2, 0.156 m/s^2] with a uniform distribution. This falling into the CL1 comfort class which requires the maximum vertical acceleration is smaller than 0.5 m/s^2. This bridge is thus considered to be satisfactory under the vibration serviceability limit state.

Comparison with residual minimization and traditional Bayesian model updating

Similar to Fort Siloso Skywalk, Equation (11) is used as the objective function for residual minimization. The optimal parameter set is E = 40 GPa, D = 2646 kg/m^3, log V_{A} = 7.60, log V_{M} = 7.96 and log L_{S} = 8.82. The method used in RM and tBMU is the same as the ones used in Fort Siloso Skywalk. The uncertainties used in tBMU are also following the same rule in Fort Siloso Skywalk. Figure 14 shows that the ranges of the posterior distribution using traditional BMU (blue histogram) are larger than the parameter range obtained using EDMF (pink area). This is because compared with traditional BMU, EDMF accounts for the biased uncertainty. As a result, EDMF is able to narrow the ranges of the parameter values.

Figure 15 presents the predicted maximum acceleration using the identification results of the three methods. The prediction by the optimal parameter set using RM is 0.121 m/s^2. Traditional BMU gives a much larger range than EDMF. The 5$^{\text{th}}$ and 95$^{\text{th}}$ percentile range of the traditional BMU (0.110 m/s^2 to 0.268 m/s^2) is 3.4 times of the ranges calculated using EDMF (0.109m/s^2 to 0.156 m/s^2). This is because EDMF includes biased uncertainty in the identification process, but traditional BMU is unable to do so. As a result, the predictions by EDMF identification results are much narrower than the predictions by the traditional BMU.

Cross validation is also carried out for RM and BMU to evaluate their accuracy in structural identification. The results are shown in Figure 16. In all scenarios except Scenario 3, RM's predictions are far away from the measurements. In Scenario 3, RM's prediction is close to but still outside the measurement bounds. Thus, RM fails to predict the "unknown" mode in all scenarios. In Scenario 1 and Scenario 5, tBMU's predictions (blue histogram) are outside the measurement bounds, failing to predict the correct value of $f1$ and $f5$. The conclusions are summarized in Table 14. In this case study, Both RM and tBMU fails to pass cross validation while EDMF is validated. In this case, the identification results obtained by RM and tBMU and further predictions of maximum acceleration are not considered to be valid.

Conclusions

This paper focuses on vibration serviceability assessment for pedestrian bridges based on model falsification. Two pedestrian bridges, namely Fort Siloso Skywalk (Singapore) and Dowling Hall footbridge (USA), have been studied. The performance of model falsification has also been compared with the other two commonly used methods. The significance of using model falsification and the findings for the two case studies are summarized as follows.

- Accounting for both modeling and measurement uncertainties, model falsification is able to provide accurate parameter identification and response prediction. The assessment based on model falsification on the maximum acceleration is consistent with experimental observations. It successfully assessed the human comfort class of vibrations in two pedestrian bridges which have different critical vibration modes (lateral mode for the first case study and vertical mode for the second case study).
- The widely use method of residual minimization is unable to identify parameter values accurately in the presence of modeling and measurement uncertainties, potentially underestimating the real response of the bridge.
- Traditional Bayesian model updating with zero-mean Gaussian likelihood function is able to provide accurate parameter identification for the first case study but not for the second case study – because of biased uncertainty. This would lead to a very wide range of predictions and thus cannot provide valuable information for decision makers.

Data Availability Statement

Some or all data, models, or code generated or used during the study are proprietary or confidential in nature and may only be provided with restrictions. Specifically, direct requests for the drawings or experimental data or models for the case study of Fort Siloso Skywalk and the Dowling Hall footbridge may be made to the third party, as indicated in the Acknowledgements.

Acknowledgements

This research was conducted at the Future Cities Laboratory at the Singapore-ETH Centre (SEC). The SEC was established as a collaboration between ETH Zurich and National Research Foundation (NRF) Singapore (FI 370074016) under the NRF's Campus for Research Excellence and Technological Enterprise (CREATE) programme. The authors gratefully acknowledge the support of Prof. Babak Moaveni for generously providing the case study of Dowling Hall Footbridge, and Sentosa Development Corporation, CPG Consultants Pte. Ltd. for the case study of Fort Siloso Skywalk. The authors also thank Prof. Siu-Kui Au for his help with Bayesian operational modal analysis.

References

ANSYS. (2016). *User's manual 17.0.*

Araujo, I. G., Maldonado, E., and Cho, G. C. (2011). "Ambient vibration testing and updating of the finite element model of a simply supported beam bridge." *Frontiers of Architecture and Civil Engineering in China*, 5(3), 344.

Au, S. K. (2012a). "Fast Bayesian ambient modal identification in the frequency domain, Part I: Posterior most probable value." *Mechanical Systems and Signal Processing*, 26, 60–75.

Au, S. K. (2012b). "Fast Bayesian ambient modal identification in the frequency domain, Part II: Posterior uncertainty." *Mechanical Systems and Signal Processing*, 26, 76–90.

Au, S. K. (2017). *Operational modal analysis: Modeling, Bayesian inference, uncertainty laws. Springer*.

Beck, J. L., and Katafygiotis, L. S. (1998). "Updating models and their uncertainties. I: Bayesian statistical framework." *Journal of Engineering Mechanics*, 124(4), 455–461.

Bertola, N. J., Papadopoulou, M., Vernay, D., and Smith, I. F. C. (2017). "Optimal multi-type sensor placement for structural identification by static-load testing." *Sensors (Switzerland)*, 17(12), 2904.

Brownjohn, J. M. W., and Darby, A. (2018). "Human factors simulation for motion and servicebility in the built environment." *13th UK Conference on Wind Engineering*.

Brownjohn, J. M. W., Moyo, P., Omenzetter, P., and Lu, Y. (2003). "Assessment of highway bridge upgrading by dynamic testing and finite-element model updating." *Journal of Bridge Engineering*, 8(3), 162–172.

Brownjohn, J. M. W., De Stefano, A., Xu, Y.-L., Wenzel, H., and Aktan, A. E. (2011). "Vibration-based monitoring of civil infrastructure: challenges and successes." *Journal of Civil Structural Health Monitoring*, 1(3–4), 79–95.

Byfield, M., and Paramasivam, S. (2012). "Summary review of structural health monitoring applications for highway bridges." *Journal of Performance of Constructed Facilities*, 26(4), 371–376.

Cao, W.-J., Koh, C. G., and Smith, I. F. C. (2019a). "Enhancing static-load-test identification of bridges using dynamic data." *Engineering Structures*, 186, 410–420.

Cao, W.-J., Zhang, S., Bertola, N. J., Smith, I. F. C., and Koh, C. G. (2019b). "Time series data interpretation for ' wheel-flat ' identification including uncertainties."

Catbas, F. N., and Kijewski-Correa, T. (2013). "Structural identification of constructed systems: collective effort toward an Integrated approach that reduces barriers to adoption." *Journal of Structural Engineering*, 139(10), 1648–1652.

Cheung, S. H., and Beck, J. L. (2009). "Bayesian model updating using hybrid Monte Carlo simulation with application to structural dynamic models with many uncertain parameters." *Journal of Engineering Mechanics*, 135(4), 243–255.

Cheung, S. H., and Beck, J. L. (2010). "Calculation of posterior probabilities for Bayesian model class assessment and averaging from posterior samples based on dynamic system data." *Computer-Aided Civil and Infrastructure Engineering*, 25(5), 304–321.

Chib, S., and Greenberg, E. (1995). "Understanding the metropolis-hastings algorithm." *American Statistician*, 49(4), 327–335.

EN 1990:2002/A1:2005 Eurocode—Basis of structural design. Application for bridges. (2005). .

Exler, O., and Schittkowski, K. (2007). "A trust region SQP algorithm for mixed-integer nonlinear programming." *Optimization Letters*.

Feldmann, M., Andreas, K., Hechler, O., Waarts, P. H., Mladen, L., Smith, A., Arndt, G., Galanti, F., Heinemeyer, C., Cunha, A., Caetano, E. S., Schlaich, M., Renata, O., and Hicks, S. (2010). "Human Induced Vibraitons of Steel Structures (HiVoSS)." *Office for Official Publications of the European Communities, Luxembourg*.

Friswell, M. I., Penny, J. E. T., and Garvey, S. D. (1998). "A combined genetic and eigensensitivity algorithm for the location of damage in structures." *Computers and Structures*.

Goller, B., Beck, J. L., and Schuëller, G. I. (2012). "Evidence-based identification of weighting factors in Bayesian model updating using modal data." *Journal of Engineering Mechanics*, 138(5), 430–440.

Goulet, J.-A., Kripakaran, P., and Smith, I. F. C. (2010). "Multimodel structural performance monitoring." *Journal of Structural Engineering*, 136(10), 1309–1318.

Goulet, J.-A., Michel, C., and Smith, I. F. C. (2013). "Hybrid probabilities and error-domain structural identification using ambient vibration monitoring." *Mechanical Systems and Signal Processing*, Elsevier, 37(1–2), 199–212.

Goulet, J.-A., and Smith, I. F. C. (2013). "Structural identification with systematic errors and unknown uncertainty dependencies." *Computers and Structures*, 128, 251–258.

Goulet, J.-A., Texier, M., Michel, C., Smith, I. F. C., and Chouinard, L. (2014). "Quantifying the effects of modeling simplifications for structural identification of bridges." *Journal of Bridge Engineering*, 19(1), 59–71.

Goulet, J. A. (2012). (2012). "Probabilistic model falsification for infrastructure diagnosis." *EPFL Thesis No 5417. Lausanne: Swiss Federal Institute of Technology (EPFL)*.

Jaynes, E. T. (2003). *Probability Theory: The Logic of Science*. *Cambridge University Press*.

Kim, G. H., and Park, Y. S. (2004). "An improved updating parameter selection method and finite element model update using multiobjective optimisation technique." *Mechanical Systems and Signal Processing*.

L. S. Katafygiotis; J. L. Beck. (1998). "Updating models and their uncertainties. II: Model identifiability." *Journal of Engineering Mechanics*, 124(4)(April), 463–467.

Lam, H. F., Yang, J., and Au, S. K. (2015). "Bayesian model updating of a coupled-slab system using field test data utilizing an enhanced Markov chain Monte Carlo simulation algorithm." *Engineering Structures*, 102, 144–155.

Lee, H.-H. (2018). *Finite element simulations with ANSYS Workbench 19*. *SDC publications*.

Liu, W.-S., and Cheung, S. H. (2020). "Decoupled reliability-based geotechnical design of deep excavations of soil with spatial variability." *Applied Mathematical Modelling*, 85, 46–59.

Moaveni, B., and Behmanesh, I. (2012). "Effects of changing ambient temperature on finite element model updating of the Dowling Hall Footbridge." *Engineering Structures*, Elsevier Ltd, 43, 58–68.

Moser, G., Paal, S. G., and Smith, I. F. C. (2018). "Leak detection of water supply networks using error-domain model falsification." *Journal of Computing in Civil Engineering*, 32(2), 04017077.

Moser, P., and Moaveni, B. (2013). "Design and deployment of a continuous monitoring system for the Dowling Hall footbridge." *Experimental Techniques*, 37(1), 15–26.

Mottershead, J. E., Link, M., and Friswell, M. I. (2011). "The sensitivity method in finite element model updating: A tutorial." *Mechanical Systems and Signal Processing*, Elsevier, 25(7), 2275–2296.

Murray, T. M., Allen, D. E., and Ungar, E. E. (1997). *Steel design guide series 11: Floor vibrations due to human activity*. American Institute of Steel Construction, Chicago.

Nguyen, N. T., Sbartaï, Z. M., Lataste, J. F., Breysse, D., and Bos, F. (2013). "Assessing the spatial variability of concrete structures using NDT techniques - Laboratory tests and case study." *Construction and Building Materials*, (49), 240–250.

Papadopoulou, M., Raphael, B., Smith, I. F. C., and Sekhar, C. (2016). "Optimal sensor placement for time-dependent systems: application to wind studies around buildings." *Journal of Computing in Civil Engineering*, 30(2), 04015024.

Pasquier, R., D. Angelo, L., Goulet, J.-A., Acevedo, C., Nussbaumer, A., and Smith, I. F. C. (2016). "Measurement, data interpretation, and uncertainty propagation for fatigue assessments of structures." *Journal of Bridge Engineering*, 21(5), 4015087.

Pasquier, R., Goulet, J.-A., Acevedo, C., and Smith, I. F. C. (2014). "Improving fatigue evaluations of structures using in-service behavior measurement data." *Journal of Bridge Engineering*, 19(11), 04014045.

Pasquier, R., and Smith, I. F. C. (2016). "Iterative structural identification framework for evaluation of existing structures." *Engineering Structures*, 106, 179–194.

Rainieri, C., and Fabbrocino, G. (2014). *Operational Modal Analysis of Civil Engineering Structures. Springer, New York*.

Ren, W. X., and Peng, X. L. (2005). "Baseline finite element modeling of a large span cable-stayed bridge through field ambient vibration tests." *Computers and Structures*, 83(8–9), 536–550.

Yin, T., Lam, H. F., and Chow, H. M. (2010). "A Bayesian probabilistic approach for crack characterization in plate structures." *Computer-Aided Civil and Infrastructure Engineering*, 25(5), 375–386.

Yuen, K.-V., Au, S. K., and Beck, J. L. (2004). "Two-stage structural health monitoring approach for phase I benchmark studies." *Journal of Engineering Mechanics*, 130(1), 16–33.

Yuen, K.-V., Beck, J. L., and Katafygiotis, L. S. (2006). "Efficient model updating and health monitoring methodology using incomplete modal data without mode matching." *Structural Control and Health Monitoring*, 13(1), 91–107.

Zheng, W., and Yu, Y. (2013). "Bayesian probabilistic framework for damage identification of steel truss bridges under joint uncertainties." *Advances in Civil Engineering*, 2013.

Table 1: Damping ratios based on decayed vibration after jumping

Jump direction	Span	ζ (%)	R^2
Vertical	A	1.87	0.9625
	B	1.55	0.8056
	C	2.94	0.9535
		R^2-weighted	2.15
Horizontal	A	1.35	0.7662
	B	0.71	0.8665
	C	0.96	0.9251
		R^2-weighted	0.99

Table 2: Frequency band (hand-picked) for modal identification

Mode	Frequency band (Hz)		Mode	Frequency band (Hz)	
	Lower	Upper		Lower	Upper
1	0.78	1.18	7	5.26	5.66
2	1.32	1.82	8	5.60	6.00
3	1.72	2.12	9	6.24	6.4
4	2.55	2.95	10	6.73	7.13
5	3.73	4.13	11	6.98	7.38
6	4.82	5.22	12	8.06	8.46

Table 3: Summary of modal identification results

Mode	f (Hz)		Mode	f (Hz)	
	MPV	COV (%)		MPV	COV (%)
1	1.00	0.19	7	5.46	0.10
2	1.56	0.34	8	5.81	0.11
3	1.90	0.18	9	6.45	0.11
4	2.75	0.24	10	6.97	0.21
5	3.93	0.10	11	7.13	0.14
6	5.03	0.07	12	8.27	0.05

Table 4: Parameter initial ranges

Parameter	Description	Lower bound	Upper bound
E_C **(MPa)**	Young's modulus of concrete	20,000	40,000
E_S **(MPa)**	Young's modulus of steel	199,500	220,500
D_C **(kg/m^3)**	Equivalent density of the deck	2280	2520
D_S **(kg/m^3)**	Density of steel	7458	8243
log V **(N/m)**	Logarithm of the vertical stiffness of the support	8	10
log T **(N/m)**	Logarithm of the transversal stiffness of the support	7	9
log L **(N/m)**	Logarithm of the longitudinal stiffness of the support	7	9

Table 5: Uncertainty sources of natural frequencies

Uncertainty sources		Uncertainty range (%) on natural frequency
Modelling uncertainties	Model simplifications and FE method	[−5, 3]
	Mesh refinement	[0, 2]
	Additional uncertainty	[−1, 1]
Measurement uncertainties	Modal analysis results	Shown in Table 3
	Additional uncertainty	[−1, 1]

Table 6: Cross validation of structural identification (Fort Siloso Skywalk)

Scenario	"Unknown" Mode	Prediction range with uncertainty (Hz)	Validation
1	Mode 1	[0.79, 1.08]	Yes
2	Mode 2	[1.46, 1.76]	Yes
3	Mode 3	[1.83, 2.28]	Yes
4	Mode 4	[4.69, 5.63]	Yes

5	Mode 5	[6.43, 7.55]	Yes
6	Mode 6	[7.21, 8.68]	Yes

Table 7: Modelling uncertainties of maximum accelerations (Fort Siloso Skywalk)

Modelling uncertainty sources	Uncertainty range (%)
Model simplifications and FE method	[−5, 3]
Mesh refinement	[0, 2]
Additional uncertainty	[−1, 1]

Table 8: Peak accelerations for walking

Location	**Lateral acceleration** (mm/s^2)
Point A	67
Point B	79
Point C	69
Comfort Level	CL1

Table 9: Validation of structural identification (comparison of three methods)

Case Study	EDMF	RM	tBMU
I: Fort Siloso Skywalk	Yes	No	Yes

Table 10: Parameter initial ranges

Parameter	Description	Lower bound	Upper bound
E **(MPa)**	Young's modulus of the equivalent deck	20,000	40,000
D **(kg/m³)**	Equivalent density of the deck	2635	3565
log V_A **(N/m)**	Logarithm of the vertical stiffness of the support at the abutment	7	9
log V_M **(N/m)**	Logarithm of the vertical stiffness of the support at the middle	7	9
log L_S **(N/m)**	Logarithm of the longitudinal stiffness of bearing at the side support	7	9

Table 11: Uncertainty sources of dynamic measurements

Uncertainty source		Uncertainty range (%) on natural frequency
Modelling uncertainties	Model simplifications and FE method	[−8, 5]
	Mesh refinement	[0, 2]
	Additional uncertainty	[−1, 1]
Measurement uncertainties	Temperature and environment effects	Referenced from (Moser and Moaveni 2013)
	Additional uncertainty	[−1,1]

Table 12: Identified Parameter ranges

Parameter	Lower bound	Upper bound
E **(MPa)**	25,743	39,763
D **(kg/m³)**	2640	2,953
log V_A	7.08	8.77
log V_M	7.79	8.94

log *L*s	7.87	8.97

Table 13: Cross validation of structural identification (Dowling Hall footbridge)

Scenario	"Unknown" mode	Prediction range with uncertainty (Hz)	Validation
1	Mode 1	[4.58, 5.96]	Yes
2	Mode 2	[5.73, 7.55]	Yes
3	Mode 3	[6.21, 8.07]	Yes
4	Mode 4	[7.02, 10.35]	Yes
5	Mode 5	[10.30, 13.71]	Yes
6	Mode 6	[12.02, 16.13]	Yes

Table 14: Cross validation of structural identification (comparison of three methods)

Case Study	EDMF	RM	tBMU
II: Dowling Hall Footbridge	Yes	No	No

List of figure captions

15. Figure 15: Maximum vertical accelerations predicted using RM, tBMU and EDMF (the Dowling Hall footbridge)
16. Figure 16: Cross validation results of EDMF, tBMU and RM for the Dowling Hall Footbridge: (I) Scenario 1; (II) Scenario 2; (III) Scenario 3; (IV) Scenario 4; (V) Scenario 5; (VI) Scenario 6

Figure 1: Photo of Fort Siloso Skywalk

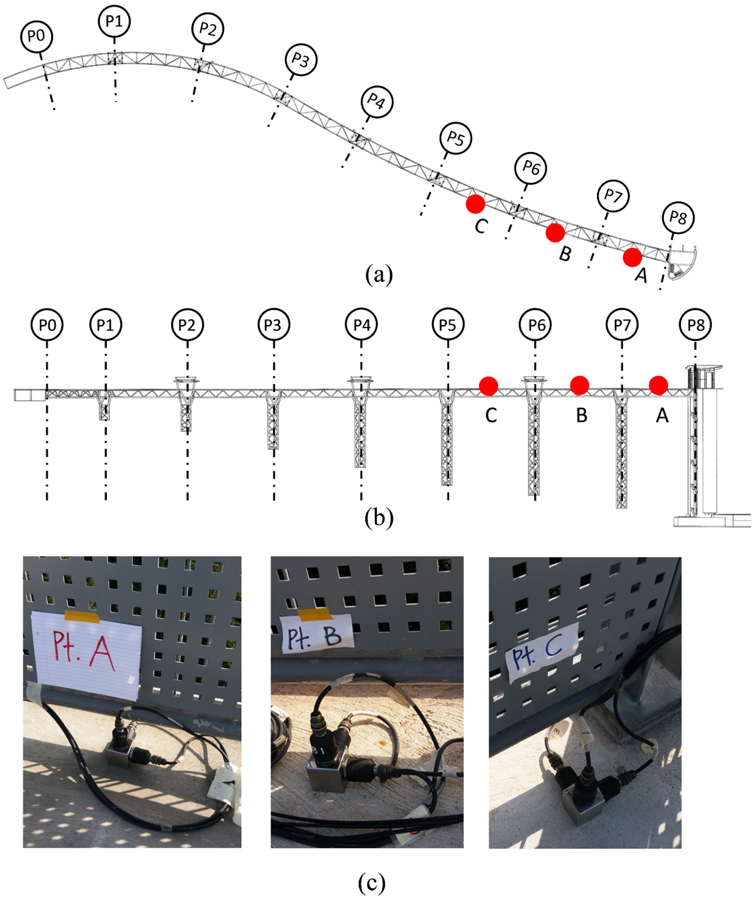

Figure 2: Configuration and photos of accelerometers: (a) plan view; (b) elevation view; (c) accelerometers installed at location A-C

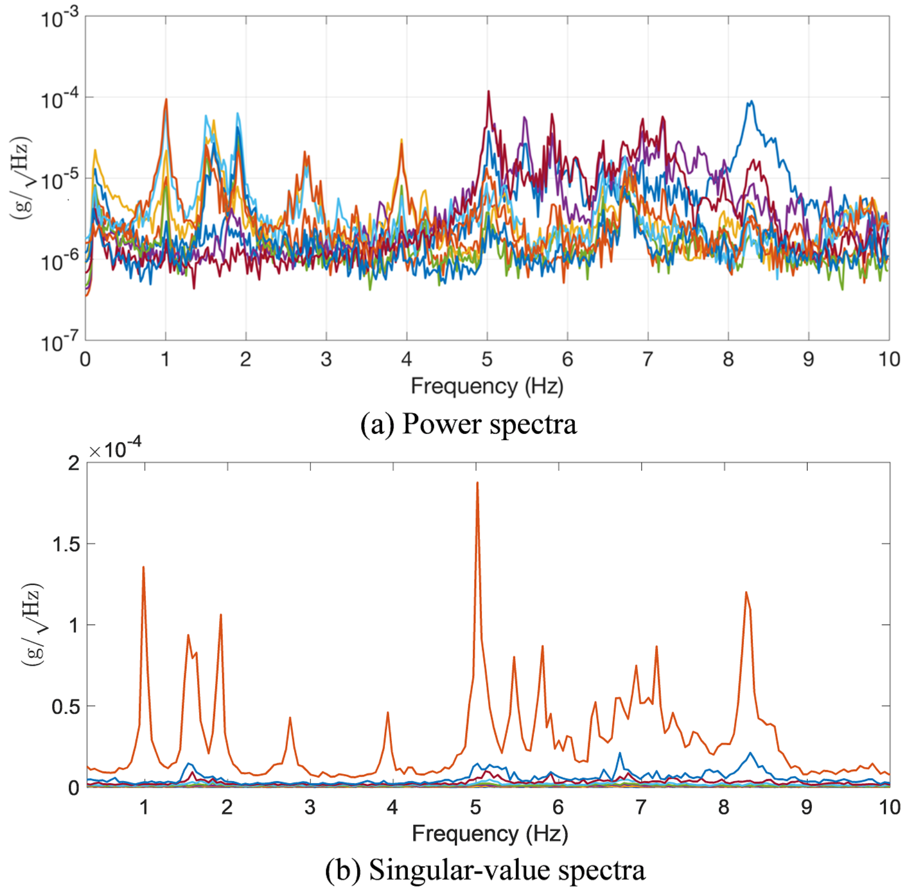

(a) Power spectra

(b) Singular-value spectra

Figure 3: (a) Power spectra; (b) singular-value spectra

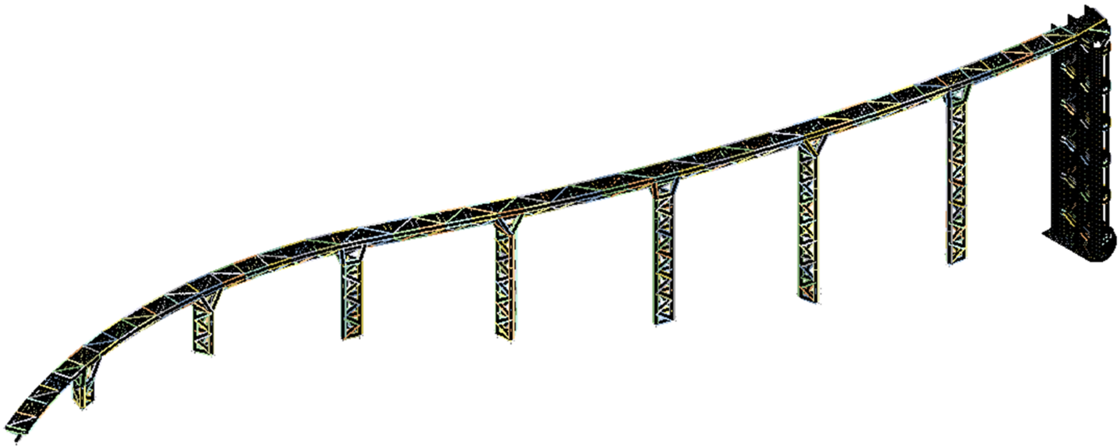

Figure 4: Finite element of Fort Siloso Skywalk

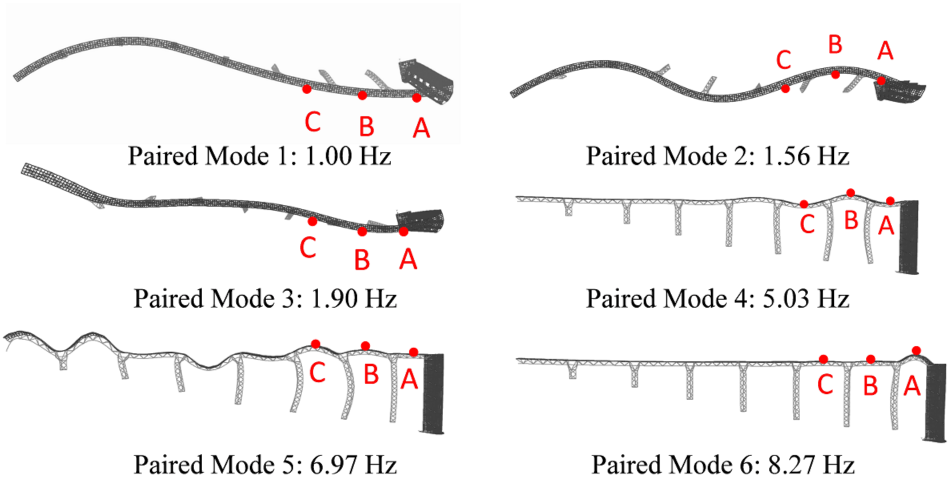

Figure 5: Paired modes

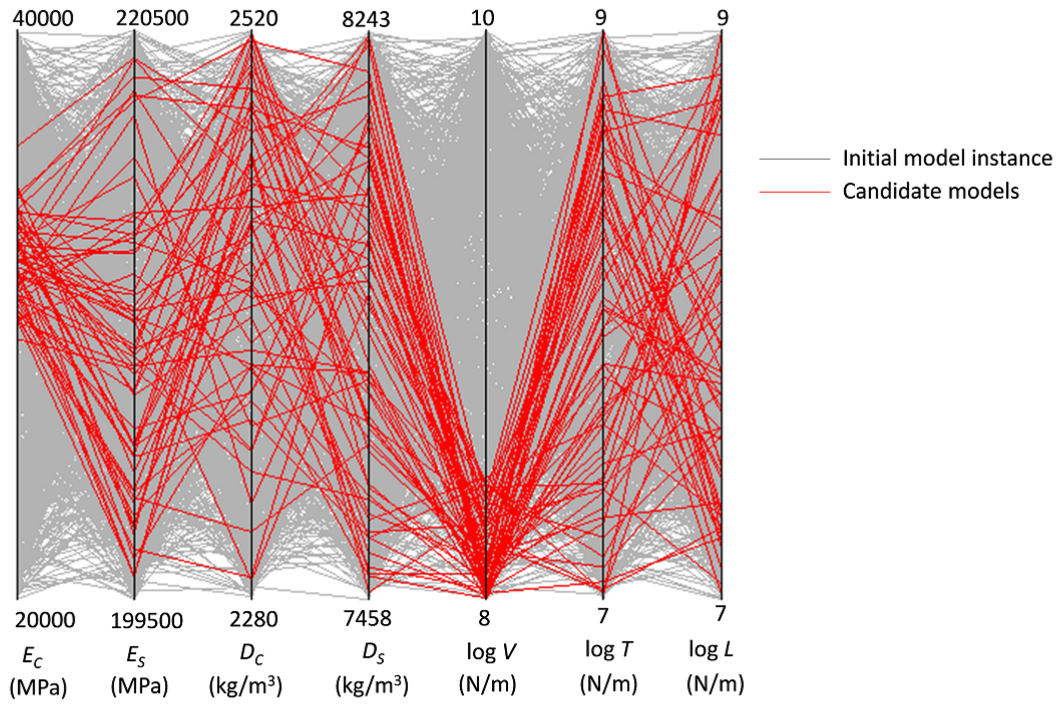

Figure 6: Candidate models of Fort Siloso Skywalk

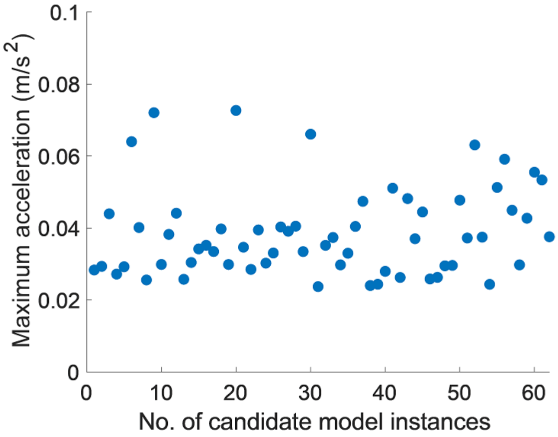

Figure 7: Maximum acceleration under lateral excitation using CMS (Fort Siloso Skywalk)

Figure 8: Photo of random walking test

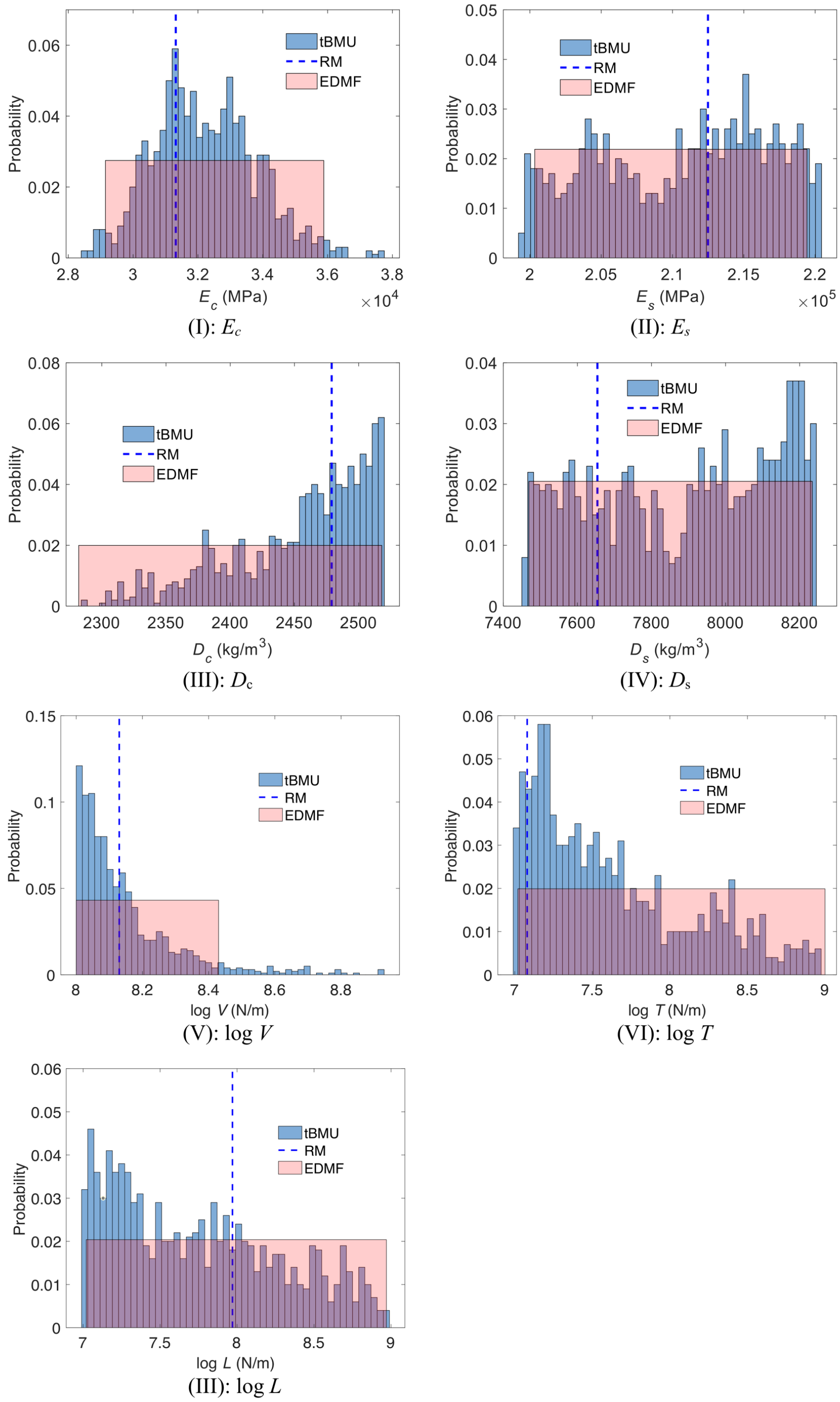

Figure 9: Posterior distribution of parameter values obtained using tBMU (blue histogram), EDMF (pink area) and residual minimization (blue dashed line) (Fort Siloso Skywalk): (I) E_c; (II) E_s; (III) D_c; (IV) D_s; (V) log V; (VI) log T; (VII) log L

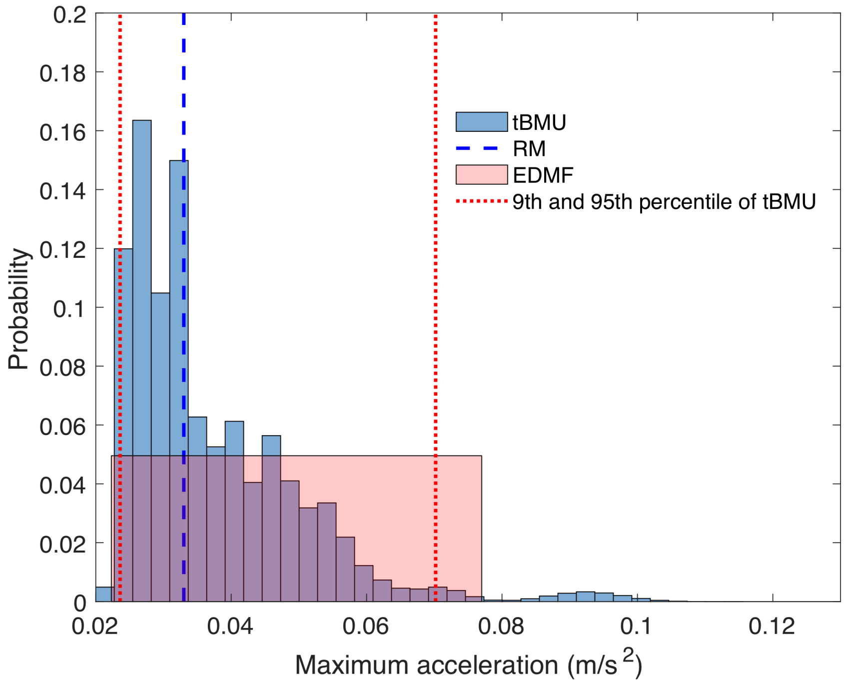

Figure 10: Maximum lateral accelerations predicted using tBMU, EDMF and residual minimization (RM) (Fort Siloso Skywalk)

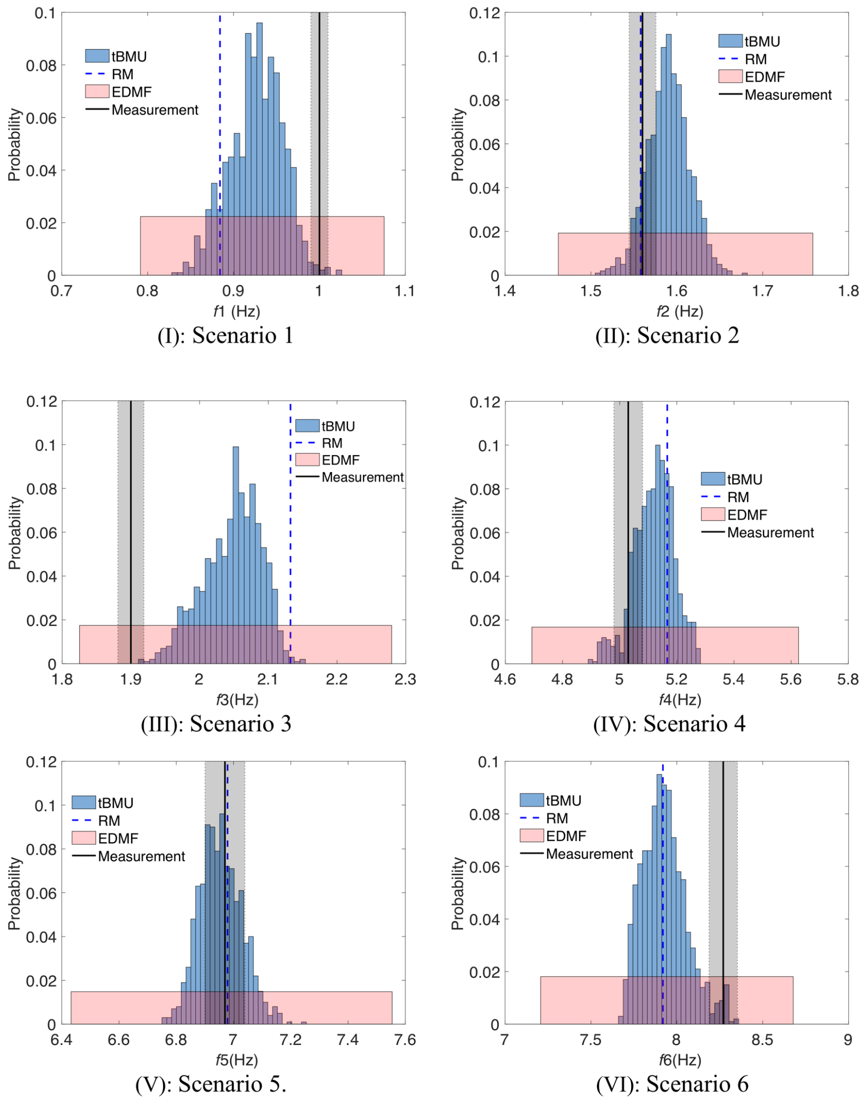

Figure 11: Cross validation results of EDMF, tBMU and RM for Fort Siloso Skywalk: (I) Scenario 1; (II) Scenario 2; (III) Scenario 3; (IV) Scenario 4; (V) Scenario 5; (VI) Scenario 6

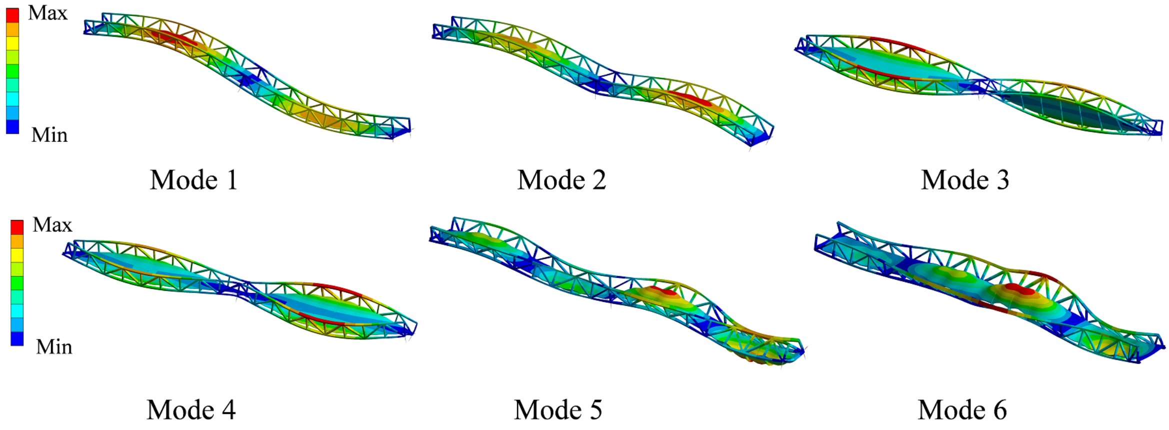

Figure 12: Results of modal analysis in ANSYS for the Dowling Hall footbridge

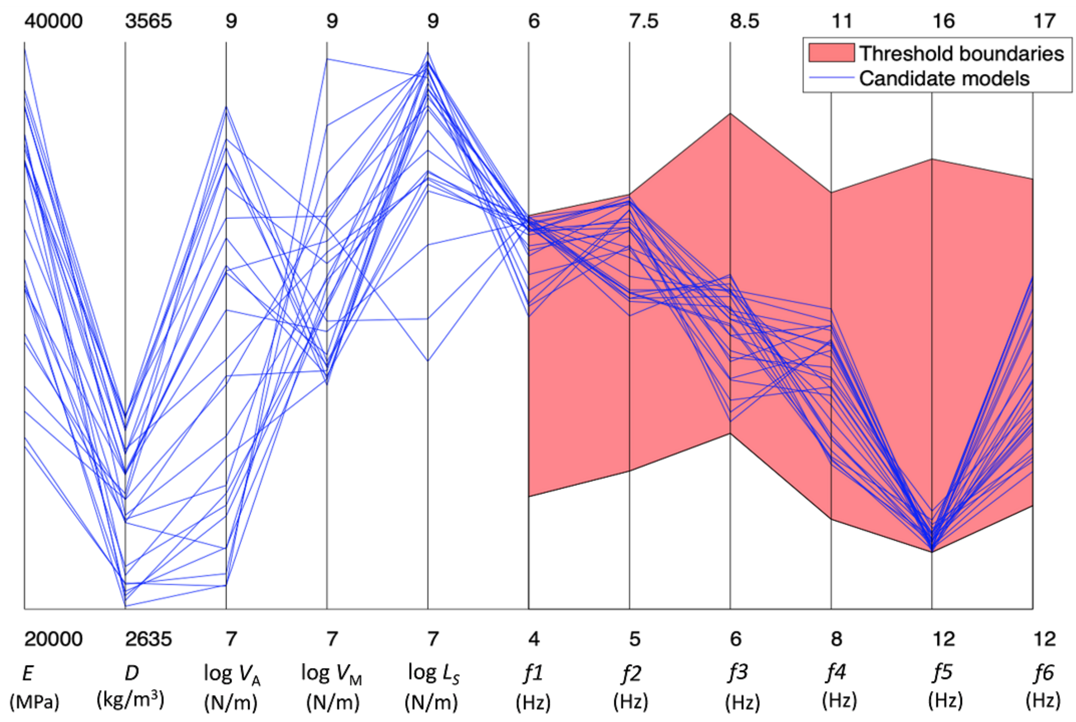

Figure 13: Candidate models of the Dowling Hall footbridge

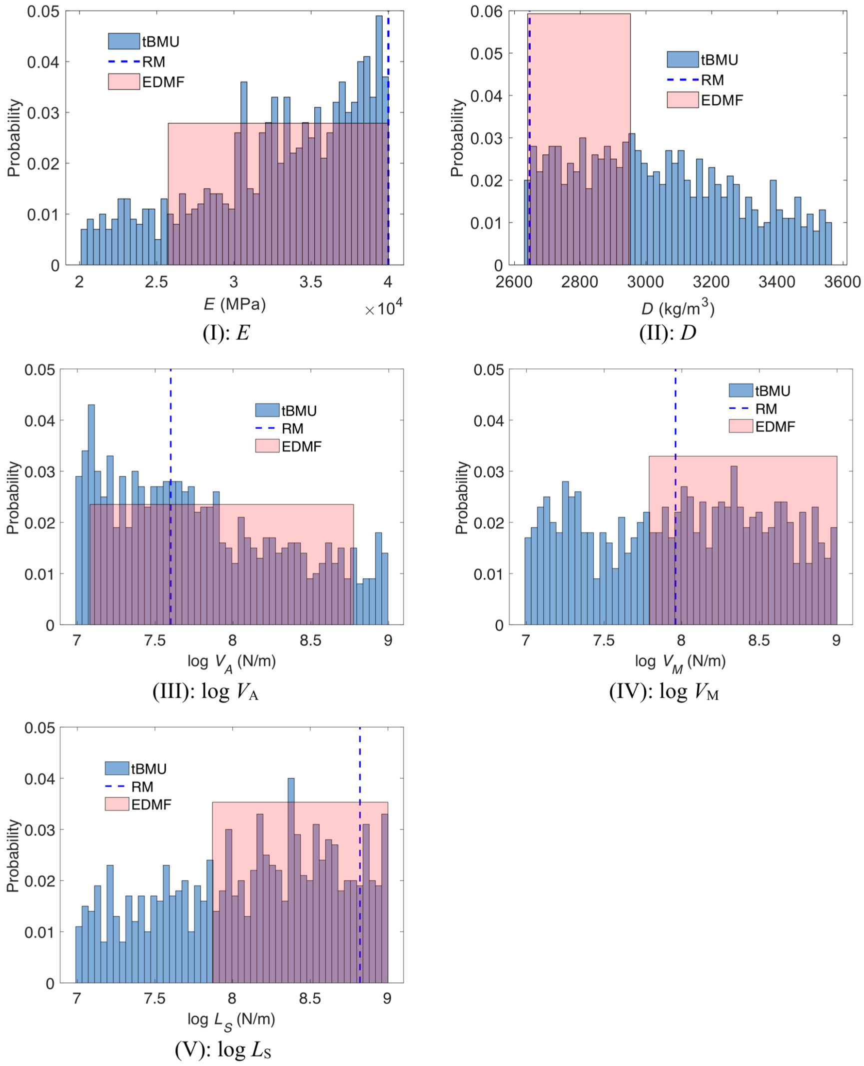

Figure 14: Posterior distribution of parameter values obtained using tBMU (blue histogram), EDMF (pink area) and residual minimization (blue dashed line) (the Dowling Hall footbridge) : (I) E; (II) D; (III) log V_{A}; (IV) log V_{M}; (V) log L_{S}

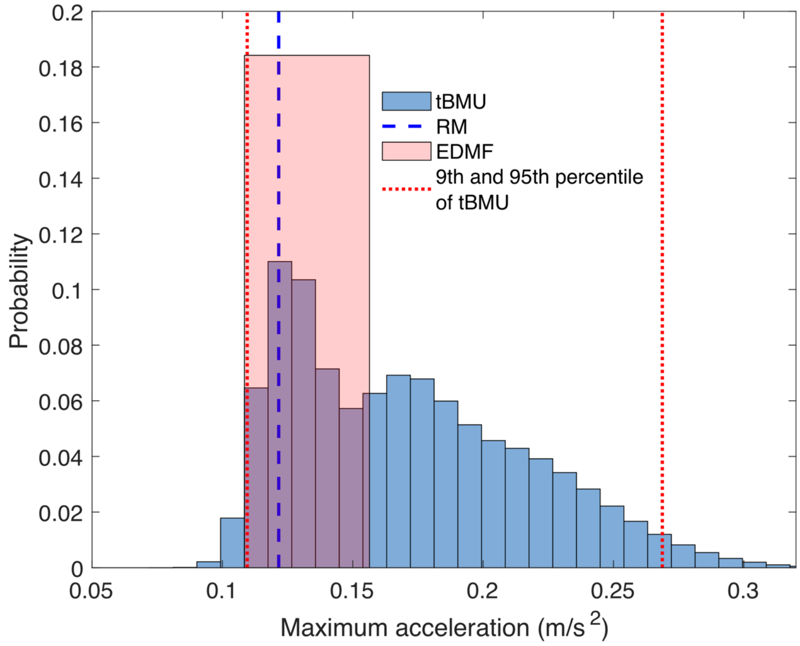

Figure 15: Maximum vertical accelerations predicted using RM, tBMU and EDMF (the Dowling Hall footbridge)

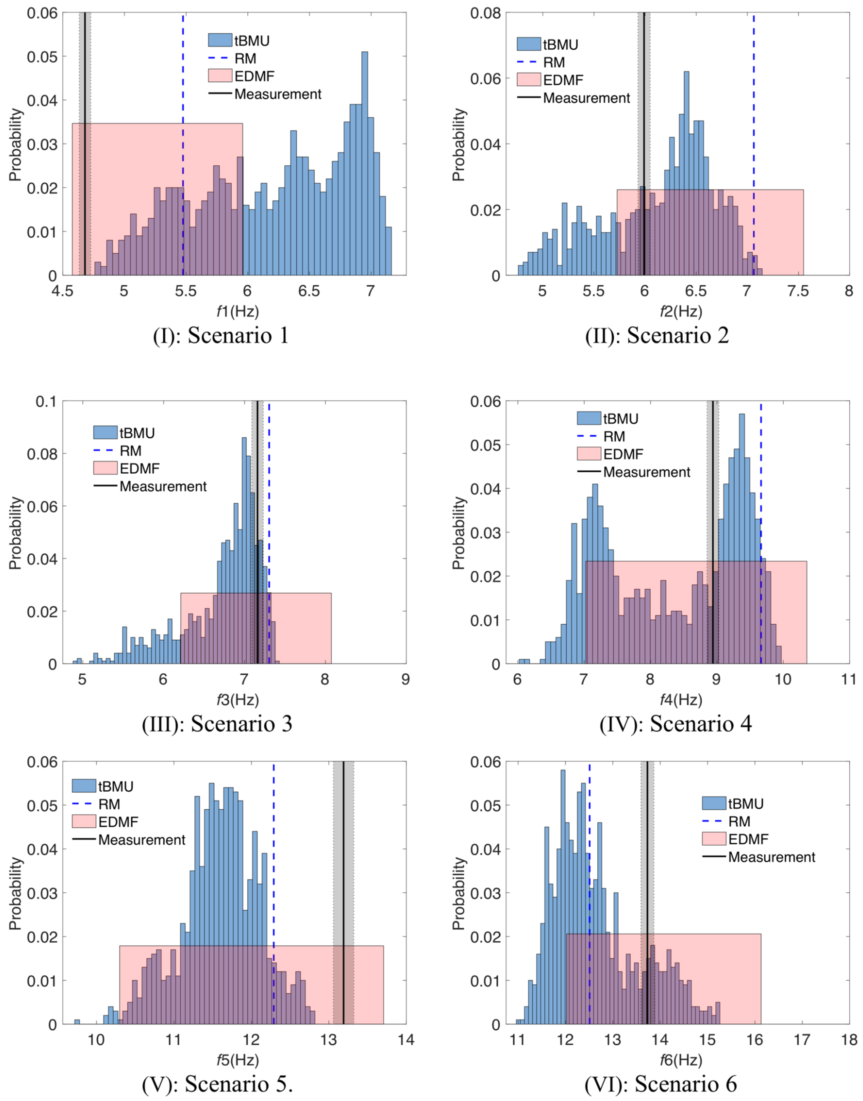

Figure 16: Cross validation results of EDMF, tBMU and RM for the Dowling Hall Footbridge: (I) Scenario 1; (II) Scenario 2; (III) Scenario 3; (IV) Scenario 4; (V) Scenario 5; (VI) Scenario 6